TiO2-graphene/chitosan nanocomposite: preparation and its application for removal of anionic dyes

Article · January 2020

DOI: 10.33945/SAMI/AJGC/2020.1.2

2 authors:

Robab Mohammadi

41 PUBLICATIONS **462** CITATIONS

SEE PROFILE

Nasrin Sabourmoghaddam

Payame Noor University

17 PUBLICATIONS **46** CITATIONS

SEE PROFILE

Asian Journal of Green Chemistry 4 (2020) 11-32

Asian Journal of Green Chemistry

Journal homepage: www.ajgreenchem.com

Orginal Research Article

TiO_2-graphene/chitosan nanocomposite: preparation and its application for removal of anionic dyes

Robab Mohammadi[a,*], Nasrin Sabourmoghaddam[b]

[a] *Department of Chemistry, Payame Noor University, PO box 19395-3697, Tehran, Iran*

[b] *Department of Environment and Natural Resources, Payame Noor University, P.O. Box 19395-3697 Tehran, Iran*

ARTICLE INFORMATION

Received: 1 December 2018
Received in revised: 8 January 2019
Accepted: 12 January 2019
Available online: 3 March 2019

DOI: 10.33945/SAMI/AJGC/2020.1.2

KEYWORDS

TiO_2-graphene/chitosan nanocomposite
Photocatalytic activity
Anionic dye
Artificial neural network
Removal efficiency

ABSTRACT

In this work, TiO_2-graphene/chitosan nanocomposite with high photocatalytic activity was successfully synthesized and characterized by various analyses such as XRD, TEM, SEM, EDX and DRS. The photocatalytic activity was tested vs. removal of methyl red as ananionic dye under black light radiation. Based on the results, TiO_2-graphene/chitosan nanocomposite could effectively remove methyl red, and demonstrate an excellent photocatalytic enhancement over TiO_2 and TiO_2-graphene samples. The degradation reaction fit well to a Langmuir-Hinshelwood kinetic model implying that the reaction rate is depended on the initial adsorption step. An artificial neural network (ANN) comprising four input variables (TiO_2-graphene/chitosan dosage, initial dye concentration, reaction time and temperature of the solution), eight neurons and an output variable (Removal efficiency %) was optimized, tested and validated for methyl red degradation by the prepared TiO_2-graphene/chitosan nanocomposite. The results showed that the predicted data from the designed ANN model are in good agreement with the experimental data with a correlation coefficient (R^2) of 0.9831. Based on the results, reaction time is the most influential variable and the temperature of solution is the less influential parameter in the removal efficiency of methyl red.

Corresponding author, email: r.mohammadi@pnu.ac.ir (R. Mohammadi).
Tel.: +9891 41192201; Fax: +9861 34417174.

Graphical Abstract

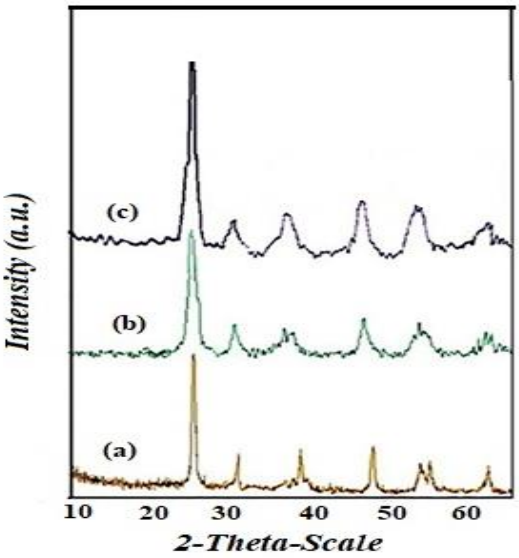

Introduction

Semiconductor-based heterogeneous photocatalysis is one of the most promising procedures for the removal of pollutants from wastewater. Among different semiconducting materials, titanium dioxide (TiO_2) presents the most suitable properties: it is chemically and biologically inert, stable, non-toxic, cheap and easy to produce [1]. However, TiO_2 has its own disadvantage that includes the fast recombination of photogenerated electron–hole pairs [2]. In order to suppress charge recombination and extend light absorption of TiO_2, many strategies have been attempted to dope TiO_2 and to combine TiO_2 with the related materials. Especially, carbon-based materials, such as carbon nano-tube, active carbon, and graphene were widely useded to modify TiO_2 [3–5].

TiO_2–graphene composites have attracted extensive attention for the different applications, including the removal of organic pollutants, generation of H_2 by water splitting, reduction of CO_2 for solar fuel production, and so on [6–8]. These research simply that the contact of TiO_2 with graphene can improve the photoactivity as compared to the bare TiO_2 and due to the enhanced adsorption of pollutants, extended light absorption range and increased charge separation [9, 10]. Graphene has a conjugated structure and its combination with TiO_2 can be an ideal preference to achieve an enhanced charge separation in electron-transfer process [11]. *Das* et al., [12] deposited various nanoparticles such as ZnO, TiO_2, Fe_3O_4 and Ni on graphene. By using first principle calculations, they showed that charge transfer occurs between graphene and the deposited nanoparticles. Sonophototcatalytic activity of Pt doped GO-TiO_2 composites for DBS degradation was carried out by *Neppolian* et al., [13]. However, the obligation to separate the nanoparticles from the suspension after

treatment restricts the procedure development. The above problems can be prevented by immobilization of the nanoparticles over appropriate supports [14].

The usage of polymeric matrixes such as alginate, chitosanand different resins is one of the most widely applied methods for the immobilization. Chitosan is a suitable natural biopolymer for the immobilization procedure due to its hydrophilicity, biodegradability, non-toxicity and availability [15]. Also, adsorption capacity of the chitosan for sequestering anionic dyes such as methyl red because of the electrostatic attraction between the protonated amine groups on the chitosan and the sulfonic groups of the anionic dyes is beneficial to increase the adsorption of anionic dyes together with the immobilized adsorbent [16].

The purpose of this work was to prepare TiO_2-graphene/chitosan nanocomposite and evaluate its photoactivity for the removal of anionic dyes such as methyl red from aqueous solutions. Also, the influence of various operational parameters such as photocatalyst dosage, initial dye concentration, reaction time, and temperature of the solution were investigated. The photocatalytic removal of methyl red in the presence of TiO_2-graphene/chitosan nanocomposite was also investigated and discussed in terms of the Langmuir–Hinshelwood kinetic model. The relative importance of each factor was calculated based on the connection weights of ANN model.

Experimental

Materials and methods

Titanium n-butoxide (TBOT), ethanol of absolute grade, graphite powder (purity 99.999%), nitric acid, sulfuric acid, potassium chlorate and methyl red were purchased from Merck Co (Germany). Chitosan, which was of analytical grade, was purchased from Sigmae Aldrich, USA. TiO_2 nanoparticles were prepared by sol-gel method according to our previous work [17].

Preparation of graphene oxide sample

According to reference [18], graphene oxide was prepared via Staudenmaier method. First, 5 g graphite was mixed with concentrated nitric acid (45 mL) and sulfuric acid (90 mL) and stirred vigorously for 20 min to get dispersion. Next, potassium chlorate (55 g) was slowly added over 30 min, to avoid sudden increases in temperature**,** and the reaction mixture was stirred for 72 h at room temperature. The mixture was then added into a copious amount of distilled water and then filtered. The obtained graphite oxide solid was rinsed repeatedly and washed with a 5% solution of HCl, and water repeatedly until the pH of the filtrate was neutral. The graphite oxide thus obtained was placed in a quartz boat and inserted into a tubular furnace preheated to 1050 °C and kept at this temperature for 30 s.

Preparation of TiO_2/GO sample

In our previous work, we reported the preparation of TiO_2/GO catalyst via hydrothermal process [19]. Graphene oxide (20 mg) was dissolved in a solution of distilled water (80 mL) and ethanol (40 mL) *via* ultrasonic treatment for 2 h. TiO_2 (200 mg) was added to the synthesized graphene oxide solution and stirred for further 2 h to obtain a homogeneous suspension. The suspension was then placed in a 200 mL Teflon-sealed autoclave and maintained at 120 °C for 3 h to simultaneously achieve the reduction of graphene oxide and the deposition of TiO_2 on the graphene sheets. Finally, the obtained sample was recovered via filtration, rinsed with high purity deionized water for several times, and dried at 70 °C for 12 h in the vacuum furnace.

Preparation of TiO_2-graphene/chitosan nanocomposite

According to ref. [20], tosynthesiz TiO_2-graphene/chitosan nanocomposite, first chitosan (8 g) was dissolved in 1000 mL of 1 M acetic acid and then mixed using magnetic stirre at 100 rpm for 2 h. Then, TiO_2-graphene (4 g) was added to the concentrated solution and magnetically stirred for 1 h to reach homogeneity. The resulted mixture was kept for 8 h in a stable place. The weight ratio of chitosan to TiO_2-graphene was 2:1. The mixture was added dropwise via a syringe to a 500 mL solution containing 15% NaOH and 95% ethanol. The volumetric ratio of NaOH/ethanol was 4. Then, they were stored in the solution for 24 h to allow the nanocomposite to be formed. The resulted sample was withdrawn from the solution and washed with deionized water several times to remove impurities. The obtained nanocomposite was dried in room temperature.

Characterization of TiO_2-graphene/chitosan nanocomposite

The major phase of the samples was determined using X-ray diffraction (XRD) (Siemens/D 5000) with Cu Kα radiation (0.15478 nm) in the 2θ scan range of 20-60°. Size of the prepared nanocomposite was obtained by TEM instrument (Philips CM-10 HT-100 kV). The texture and morphology of the prepared nanocomposite was measured via scanning electron microscope (SEM) (Philips XL-30ESM). The chemical composition of the synthesized nanocomposite was analyzed by an energy dispersive X-ray spectroscopy (EDX) system. Ultraviolet/visible diffuse reflectance spectra (DRS) of samples were performed by Avaspec-2048 TEC spectrometer in order to detect the band gap energy (E_g) of products which estimated *via* the following formula:

$$E_g = \frac{hc}{\lambda} = \frac{1240}{\lambda} \quad (1)$$

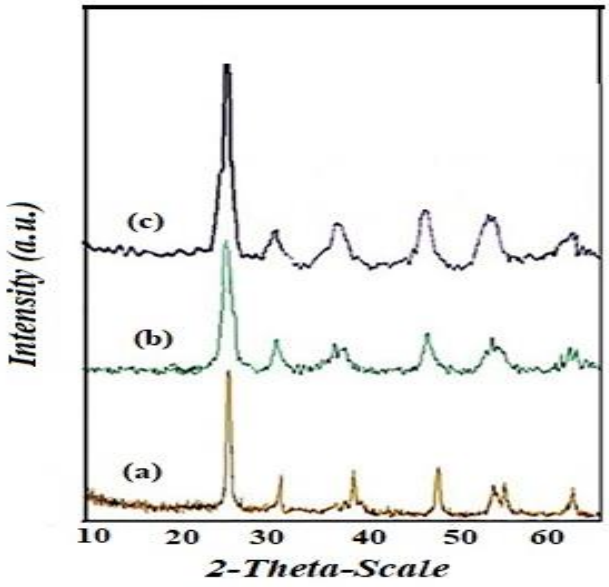

Figure 1. XRD patterns of a) TiO_2, b) TiO_2/GO and c) TiO_2-graphene/chitosan nanocomposite

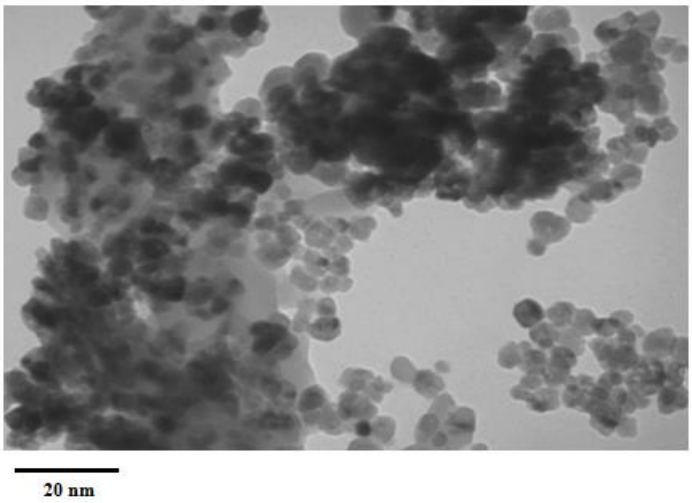

Figure 2. TEM images of TiO_2-graphene/chitosan nanocomposite

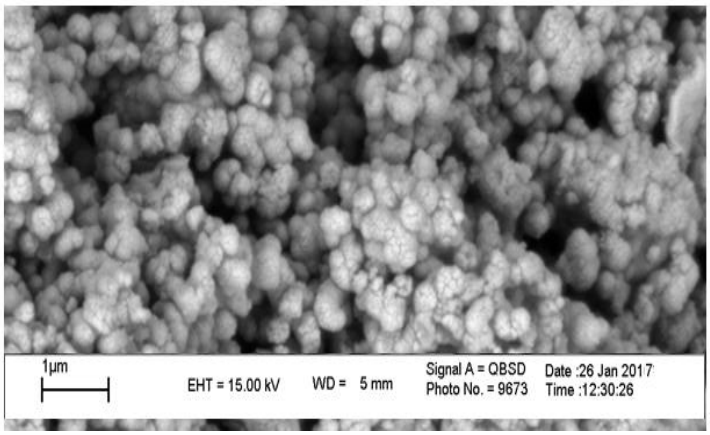

Figure 3. SEM images of TiO_2-graphene/chitosan nanocomposite

where, E_g is the band gap energy (eV), h is Planck's constant (4.1357×10^{-15} eV), c is the light velocity (2.998×10^8 m s^{-1}) and λ is the wavelength (nm).

Studies and analysis

The photocatalytic activity of the prepared samples was evaluated in the removal of model compound methyl red. The photocatalytic removal of methyl red was measured at ambient pressure and room temperature in a batch quartz reactor. Artificial illumination was provided by 36 W (UV-A) mercury lamp (Philips, Holland) with a wavelength peak at 365 nm positioned above the photoreactor. In each run, desired amounts of prepared sample and methyl red were fed into the batch quartz reactor and placed in the dark condition for 30 min with continuous stirring for adsorption–desorption equilibrium and then exposed to black-light irradiation. The zero time reading was obtained from blank solution kept in the dark. The photocatalytic reaction was then started *via* irradiating the suspension with black light. At given irradiation time intervals, 5 mL of the dye suspension was withdrawn and centrifuged to remove catalyst particles. The concentration of remaining methyl red was determined by UV–vis Perkin-Elmer 550 SE spectrophotometer at wavelengths of 410 nm. The equation used to estimate the photocatalytic removal efficiency in the treatment experiments was:

$$Removal\ efficiency\ \% = \frac{C_0 - C_t}{C_0} \times 100 \qquad (2)$$

where C_0 is the initial concentration of dye (mg/L^{-1}) and C_t isthe final concentration of dye (mg/L^{-1}).

Results and Discussion

Characterization of prepared samples

X-ray diffraction

XRD pattern of TiO_2-graphene/chitosan nanocomposite is shown in Figure 1. As shown in Figure 1, the diffraction peaks of prepared sample were observed at 2θ=25.43, 30.76, 37.82, 48.0, 54.5 and 63.04° correspond to reflections (101), (121), (004), (200), (105), (211). The diffraction peaks can be assigned to pure anatase phase [21]. However, no typical diffraction peaks belonging to the separate graphene are observed in the composite. The fact is that the main characteristic peak of graphene at 24.5° might be shielded by the main peak of anatase TiO_2 at 25.4°. Figure 1**c** shows XRD patterns of TiO_2-graphene/chitosan nanocomposite. It can be seen that there is no difference between XRD pattern of TiO_2-graphene/chitosan nanocomposite and XRD pattern of bare TiO_2, which

reveals TiO_2-graphene/chitosan nanocomposite synthesis did not destroy the characteristic structure of TiO_2. This result is similar to what was reported by Alagumuthu and Anantha Kumar [22].

TEM analysis of TiO_2 -graphene/chitosan nanocomposite

TEM image of TiO_2-graphene/chitosan nanocomposite has been illusterated in Figure 2. The average size of the primary particles estimated from TEM image is about 8-10 nm. It can be seen that the particles demonsterate a relatively uniform particle size distribution. The degree of agglomeration can be prevented through the growth of TiO_2 nanoparticles from carboxyl groups on the surface of graphene nanosheets. Therefore, graphene nanosheets can facilitate uniform dispersion of the nanoparticles on its surfaceas concluded by *Loh* et al., [23]. As shown in TEM image, chitosan layers on the TiO_2 surface attached together and generated the porous structure. The porous structure of chitosanon the TiO_2 surface and elsewhere is an important characteristic that allows specific interactions of TiO_2-graphene/chitosan nanocomposite with methyl red molecules, making it an important feature for the photocatalytic and adsorption performances [24].

SEM analysis of TiO_2-graphene/chitosan nanocomposite

SEM image of TiO_2-graphene/chitosan nanocomposite is shown in Figure 3. Figure 3 implies that TiO_2-graphene/chitosan nanocomposite has a highly porous structure which suggests the appropriate of the nanocomposite as adsorbent for removal of dye molecules from aqueous solution. *Nawi* et al. reported the fabrication of bilayer system consisting of TiO_2 and chitosan (CS) biopolymer. They found that the highly porous structure of immobilized TiO_2 layer allows better diffusion of pollutants, increases the light penetration and improves the optical property [25].

Elemental analysis with EDX spectroscopy

The elemental composition of the synthesized nanocomposite was determined using energy dispersive X-ray spectroscopy analysis. C, O, N, and Ti peaks can be clearly observed from Figure 4. EDX analysis demonstrated no significant levels of impurities which could have originated from the procedure. This result is similar to what was reported by *Hasmath Farzana* and *Meenakshi* [26].

DRS analysis

In order to investigate the influence of graphene oxide and chitosan on the optical absorption properties of titanium dioxide, DRS analysis has been performed (Figure 5). The reflectance spectra of TiO_2, and TiO_2/GO, show absorption thresholds at 390, and 415 nm, respectively, and E_g values

estimated from the Eq. 1 are 3.17, and 2.98 eV, respectively (are not shown for TiO_2). Therefore, graphene sheets narrow the band gap of TiO_2. Martinsa et al. showed that TiO_2/GO samples have lower band gap (Ranging from 2.94 to 2.35 eV) compared with pure TiO_2 (3.08 eV) [27]. These phenomenon result not only from the high conductivity of graphene that can facilitate separation of photogenerated e^-/h^+ pairs, but also from the formation of Ti–O–C bonding between TiO_2 and graphene sheets [28]. Also, this can be attributed to the charge transfer between conduction band of TiO_2 and graphene sheets. However, the electron transition from the valence band to the conduction band can occur easier with the band-gap narrowing in TiO_2 nanoparticles [29]. Furtheremore, the band gap energy (E_g) of TiO_2-graphene/chitosan nanocomposite is 2.75 eV. It can be concluded that chitosan induces band-gap narrowing in TiO_2/GOcatalyst. This can be related to the coordination of TiO_2 with the nitrogen atom. Therefore, TiO_2-graphene/chitosan nanocomposite can be excited *via* absorbing both UV and visible lights to generate more electron–hole pairs and give a maximum visible light harvesting.

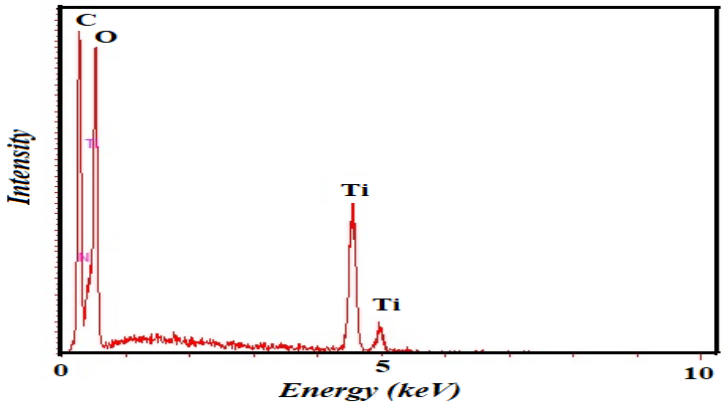

Figure 4. EDX pattern of TiO_2-graphene/chitosan nanocomposite

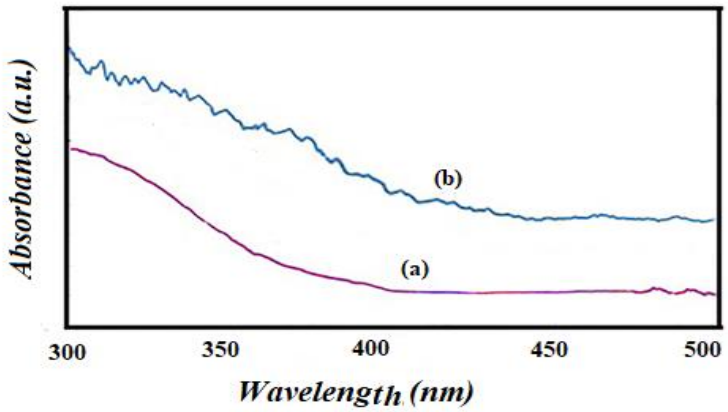

Figure 5. UV–vis DRS spectra of a) TiO_2/GO and b) TiO_2-graphene/chitosan nanocomposite

Photocatalytic removal of methyl redby synthesized samples

The results of decolorization of methyl red using synthesized materials under black light illumination are shown in Figure 6. It could be observed that photoactivity of TiO_2/GO sample is more than that of TiO_2. It can be concluded that interactions between graphene and TiO_2 lead to the improvement of the photocatalytic activity. The high photocatalytic activity of TiO_2/GO catalyst can be discussed by the following several factors:

I) Conduction band position of TiO_2 is calculated to be 3 eV, and the work function of graphene is about 4.42 eV. Therefore, graphene can act as acceptor positions for photo-generated electrons from TiO_2. Under excitation, the conduction band electrons of TiO_2 are transferred to graphene. So, the recombination of photo-generated electron-hole pairs can be prevented [30]. Therefore, the improvement in photocatalytic activity of TiO_2/GO is imaginable.

II) The electrons on the graphene can be trapped by oxygen and water on the surface of TiO_2/GO catalystand produce the hydroxyl and superoxide radicals. As a result, electron–hole recombination is largely inhibited and this further facilitates the formation of more $OH\cdot$ because of the valence band of TiO_2 and the superoxide radicals anion (O_2^{-}) at the surface of catalyst, which in turn result in a rapid decolorization of methyl red [31].

From Figure 6, photocatalytic activity of TiO_2-graphene/chitosan nanocompositeis considerably higher than that of TiO_2-graphene. TiO_2-graphene/chitosan nanocomposite became all dark red in color, that is, methyl red was strongly attracted. These results, in accordance with what reported by *Hasmath Farzana* and *Meenakshi*, showed that chitosan/TiO_2 composite was preferential to TiO_2 in photodegradation of different types of dyes such as reactive red, methylene blue, and rhodamine [26]. The incorporation of TiO_2 with Ti-OH groups into chitosan with positively charged amino groups led to the grafting of these functional groups which is desirable for the adsorption of methyl red containing negatively charged carboxilic groups.

Effect of TiO_2-graphene/chitosan dosage onphotocatalytic removal of methyl red

The influence of TiO_2-graphene/chitosan dosage on the removal of methyl red has been investigated under predetermined experimental conditions with methyl red concentration of 20 mg L^{-1}, reaction time equal to 17 min at room temperature, and changing the weight of TiO_2-graphene/chitosan in range 0.05–0.6 g L^{-1}. As can be seen from Figure 7, percentage removal of methyl red was enhanced from 31.1 to 98.5% when TiO_2-graphene/chitosan dosage was raised from 0.1 to 0.45 g L^{-1}. The enhancement in the efficiency was due to an increase in the number of active siteson TiO_2-graphene/chitosan surface and light penetration of photoactivating light into the dye-photocatalyst suspension. However, increase in the catalyst dosage beyond 0.45 g L^{-1}, the rate of

decolorization slightly decreased. The decrease in percentage of dye removal may be due to the increase in opacity of the suspension, non availability of dye molecules, and the enhancement of the light reflectance, because of the excess of TiO_2-graphene/chitosan particles. *Zhang* et al., (2002) examined the dependence of the photooxidation kinetics of methylene blue on TiO_2 loading and found that the rates increase with TiO_2 loading up to a limit and then decrease to a constant value. Others (*Daneshvar* et al. 2003; *Sohrabi* and *Ghavami*, 2008) also found the same characteristics [32–34]. An amount of 0.45 g L^{-1} of TiO_2-graphene/chitosan was applied for the subsequent photocatalytic removal experiments.

Effect of initial dye concentration

The effect of change in initial dye concentration on the removal percentage in range (10–65 mg/L^{-1}) was studied via keeping other experimental conditions constant at room temperature, reaction time equal to 17 min, and 0.45 g/L^{-1} TiO_2-graphene/chitosan concentration. As can be observed from Figure 8, the removal efficiency decclines as the initial dye concentration enhances. This behavior can be expessed *via* following parameters:

By enhancing of methyl red concentration, more and more organic substances and intermediates may be adsorbed on the surface of TiO_2-graphene/chitosan, and so the reaction of pollutant molecules with photogenerated holes or hydroxyl radicals is prevented because of the lack of any direct contact between them [35].

At high concentration of methyl red, TiO_2-graphene/chitosan surface was covered mainly by dye molecules and so production of $^{\bullet}OH$ and $^{\bullet}O_2^-$ superoxide radicals was declined [36].

These results, in accordance with what reported by Sayilkan and Emre, showed that the initial concentration of dye could affect the photocatalytic activity of TiO_2/chitosan nanocomposite and the photodegradation rate decreased with increasing initial concentration of dye [37].

Kinetic analysis as function of initial dye concentration

Finding a simple rate equation, which fits the experimental rate data, is beneficial for engineering purposes. The removal of methyl red by TiO_2-graphene/chitosan nanocomposite obeys apparently pseudo-first-order kinetics at low initial dye concentration and the rate expression is given by Equation 3.

$$\ln\left(\frac{C_0}{C_t}\right) = k_{ap}\mathrm{t} \tag{3}$$

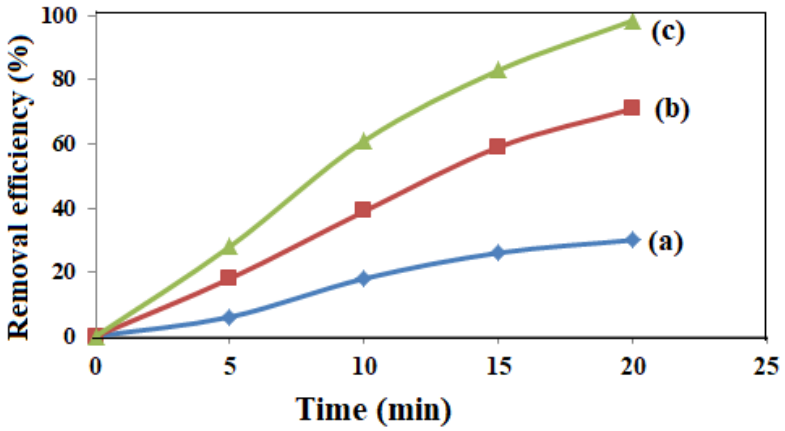

Figure 6. Photocatalytic removal of methyl red in the presence of a) TiO_2, b) TiO_2/GO, c) TiO_2-graphene/chitosan nanocomposite

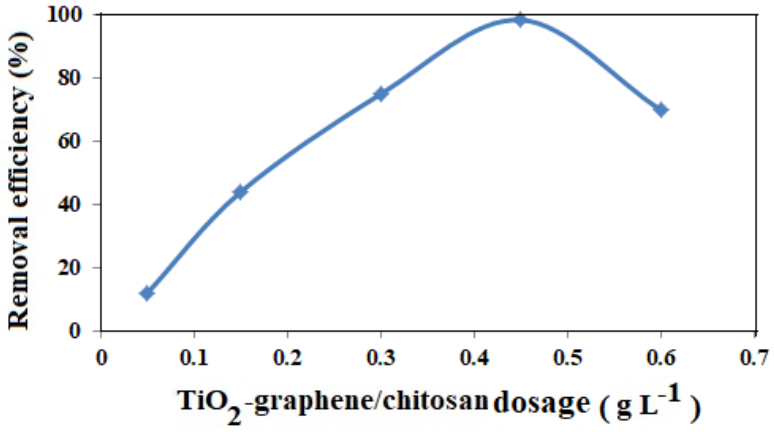

Figure 7. Effect of TiO_2-graphene/chitosan dosage on the removal efficiency of methyl red (methyl red)$_0$ = 20 mg/L^{-1}, t = 17 min, and temperature of solution = 298 K

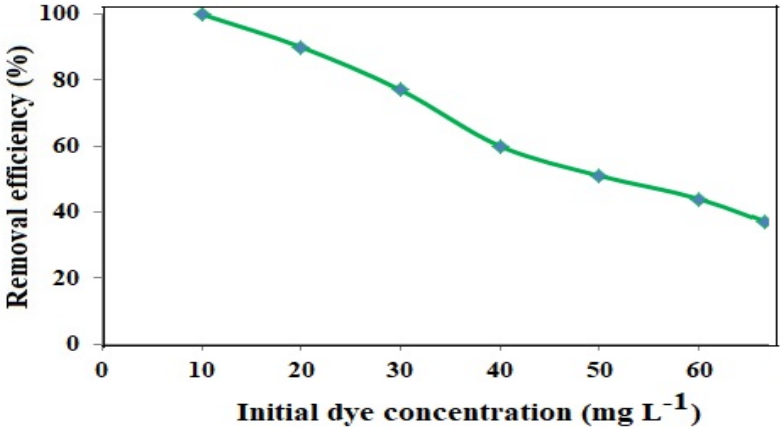

Figure 8. Effect of initial dye concentration on the removal efficiency of methyl red. [TiO_2 -graphene/chitosan]$_0$ = 0.45 g/L^{-1}, t = 17 min, and temperature of solution = 298 K

where k_{ap} is the pseudo-first-order rate constant, C_t and C_o are the concentration at time "t" and "t = 0", respectively. The values of k_{ap} can be estimated by applying a least square regression analysis. It is clear that the removal rate is dye concentration-dependent. As the concentration of methyl red was enhanced, the rate of dye removal declined. It is related to the adsorption of more dye molecules on the surface of catalyst. If more pollutant molecules are adsorbed on the surface of catalyst, the reaction of dye molecules with holes or hydroxyl radicals is prevented because of the lack of direct contact between them [38]. Furthermore, solubility of oxygen in water is low. So, during the photoreaction, oxygen concentration in the solution may be lost and photocatalytic removal efficiency decreased [39].

A few previous researchers expressed the photodegradation kinetics of organic dyes via the Langmuir-Hinshelwood (L-H) model. In order to describe the solid/liquid reaction, the experimental data have been justified in terms of the modified form of L–H kinetic model. The rate of oxidation of methyl red at surface reaction is proportional to the surface coverage of dye on TiO_2-graphene/chitosan catalyst assuming that methyl red is adsorbed on the photocatalyst surface than the intermediate products [40, 41]. Equations 4 and 5 can be used to explain the influence of initial concentration of dye on the initial degradation rate (r).

$$r = \frac{k_c k_{dye}(C)}{1 + k_{dye}(C_0)} = k_{ap}(C) \tag{4}$$

$$\frac{1}{k_{ap}} = \frac{1}{k_c k_{dye}} + \frac{C_0}{k_c} \tag{5}$$

In these equations, k_{dye} and k_c show L–H adsorption equilibrium constant and rate constant of surface reaction. Several experiments were carried out with various initial dye concentrations. The values of k_{dye} and k_c were obtained *via* the linearized equation by plotting $1/k_{ap}$ vs. $[C_0]$. From the slope of the straight line, k_c was computed equal to 3.21 mg/L^{-1} min^{-1}, while from the intercept, k_{dye} was 0.85 (mg L^{-1})$^{-1}$ for the removal of methyl red using TiO_2-graphene/chitosan nanocomposite. Mohammadi and her coworkers reported Langmuir-Hinshelwood equation constants for mineralization of amoxicillin trihydrate (AMOX) drug in the presence of Sn/TiO_2 nanoparticles. The values of K_{AMOX} and k_c were 0.56 (mg/L^{-1})$^{-1}$ and 1.86 mg/L^{-1} min^{-1}, respectively [42].

Effect of reaction time

The effect of blacklight illumination time on the photocatalytic removal of methyl red was studied from 1 to 21 min, at 20 mg/L^{-1} methyl red concentration, 0.45 g/L^{-1} catalyst concentration, and at

room temperature (Figure 9). The results showed that the percentage of methyl red removal increased with an increase of the illumination time and reached up to 98.5% after 15 min of illumination time. Such data indicates the relatively higher activity of TiO_2-graphene/chitosan enables the higher percentage of discoloration of methyl red in such short illumination time and has active sites for carrying out the reaction [43]. This result is similar to what was reported by *Wang* et al. [44].

Effect of temperature

The influence of change in reaction temperature on the removal percentage in range (293-312 K) was studied *via* keeping other experimental conditions constant at methyl red concentration of 20 mg/L^{-1}, reaction time equal to 17 min, and TiO_2-graphene/chitosan dosage of 0.45 g/L^{-1}. The results are illustrated in Figure 10. It can be observed the removal rate of methyl red increased from 88.2 to 99.1% when the temperature was increased from 293 to 313 K. *Mozia* et al., (2009) observed that an increase in solution temperature from 313 to 323 K resulted in an 11% increase in the photodegradation rate constant of acid red 18 in the presence of TiO_2 [45]. It is well known that electron-hole pair production in the presence of light source is responsible for initiation of photoreaction [46]. So, the photo decolorization systems are usually operated at room temperature.

ANN modeling

ANN is an appropriate method for its ability in learning, simulation and prediction of experimental data. The topology of an ANN can be detected *via* the number of layers, the number of nodes in each layer and the nature of the transfer functions. Optimization of ANN topology is probably the most important step in the development of a model [47]. We applied a three-layered, feed for wardback-propagation neural network in this work. The network examined in our study contained four in puts, representing TiO_2-graphene/chitosan dosage, initial methyl red concentration, reaction time, and temperature. The ranges of operational parameters are given in Table 1. The output pattern comprised one neuron representing the photocatalytic dye removal efficiency (%).

Artificial neural network used experimental data sets in different conditions to test training. The experimental data sets were split into training (1/2), validation (1/4) and test (1/4) subsets. All inputs and target data must be scaled within a specified range. So, all data (X_i) were scaled (x_i) into the 0.2-0.8 ranges, through equation 6 [48];

$$x_i = 0.2 + \frac{0.6(X_i - X_{\min})}{(X_{\max} - X_{\min})} \quad (6)$$

Figure 9. Effect of reaction time on the removal efficiency of methyl red. [TiO_2-graphene/ chitosan]$_0$ = 0.45 g L^{-1}, (methyl red)$_0$ = 20 mg/L^{-1}, and temperature of solution = 298 K

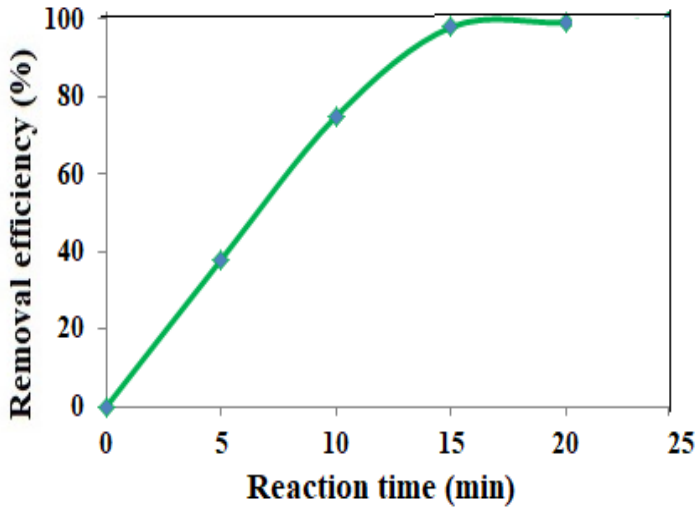

Figure 10. Effect of temperature of solution on the removal efficiency of methyl red. (TiO_2 -graphene/ chitosan)$_0$ = 0.45 g L^{-1}, (methyl red)$_0$ = 20 mg/L^{-1}, and t = 17 min

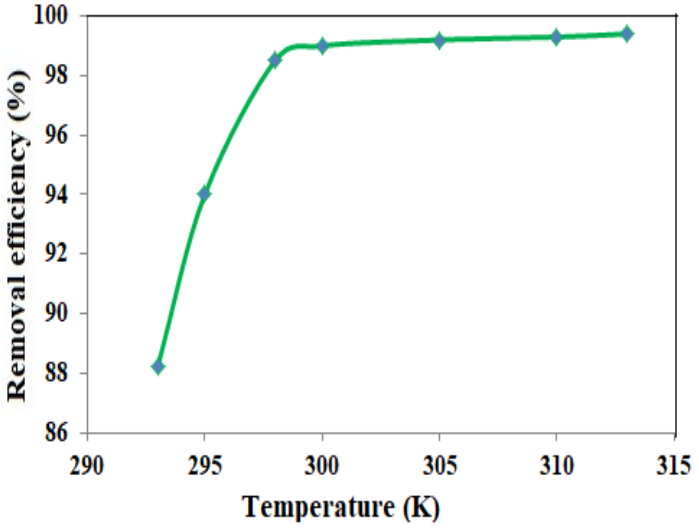

Table 1. The ranges of input and output variables

Variable	Range of the parameter value
Input layer	
TiO_2 -graphene/ chitosan dosage (g/L^{-1})	0.05-0.6
Initial dye concentration (mg/L^{-1})	10-65
Reaction time (min)	1-21
Temperature (K)	293-312
Output layer	
Removal efficiency (%)	9.2-100

where X_{min} and X_{max} refer to the lowest and the highest value of the input variable X_i, respectively. It is the hidden layer structures that essentially explain the topology of a feed-forward network. It is well known that the selection of neurons in the hidden layer may have an important effect on network performance. In our research work, we tested various numbers of neurons, from 1 to 16, in the hidden layer. Figure 10 shows the relation between the network error and the number of neurons in the hidden layer. Each topology was repeated 3 times at least to prevent random correlation due to the random initialization of the weights. Optimization was based on minimizing the mean square error, MSE, which is defined as follows:

$$MSE = \frac{\sum_{i=1}^{i=N} (t_i - a_i)^2}{N} \quad (7)$$

where t_i and a_i are the predicted and experimental data of the dependent variable, respectively and N is the number of data. The relationship between MSE and the number of neurons in the hidden layer is presented in Figure 11. As can be seen that the performance of the network stabilized after inclusion of an adequate number of hidden units just about eight; therefore, 8 neurons were selected for the best performance of neural network model. The resulting ANN is schematically illustrated in Figure 12. Figure 12 shows the optimized ANN structure characterized by one hidden layer containing eight neurons.

To test the precision of the ANN model, a comparison was made between experimental and predicted removal efficiency (%) values. Figure 13 shows a comparison between experimental and predicted values of the output for the test set, using the optimum neural network model with eight neurons in the hidden layer. The correlation coefficient (R^2) of the line indicating the best fit on the data of the scatter plot, obtained with regression analysis based on the minimization of the squared errors, is 0.9831. From this plots, it can be conclude that the results obtained from the models are in good agreement with the experimental data, and the model accurately predicts removal efficiency of methyl red under different conditions.

Figure 14 shows a comparison between predicted and experimental values of the output variable (Removal efficiency %) as a function of the initial concentration of methyl red, using the neural network model. These results confirm that the designed ANN modelis able to adequately predict the photocatalytic efficiency under different conditions, within the experimental range adopted in the model fitting.

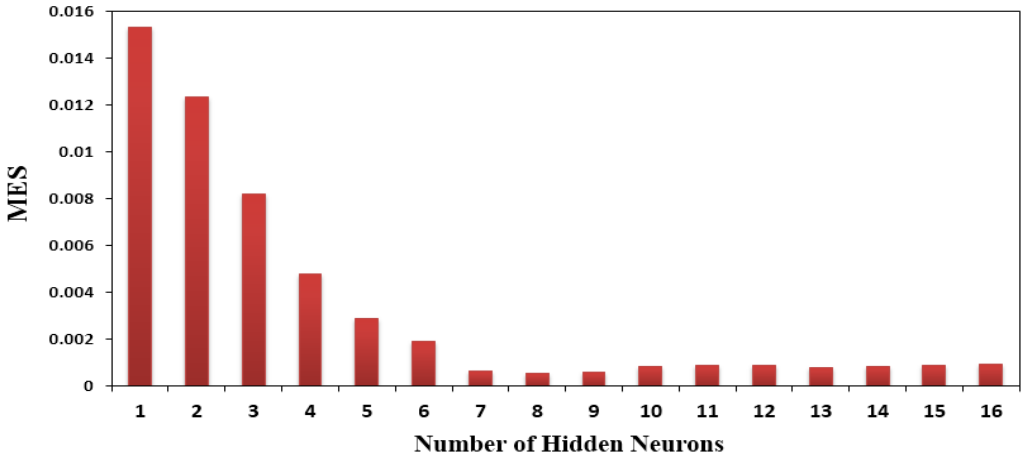

Figure 11. Effect of the number of neurons in the hidden layer on the performance of the neural network

Figure 12. Schematic illustration of the optimized ANN structure

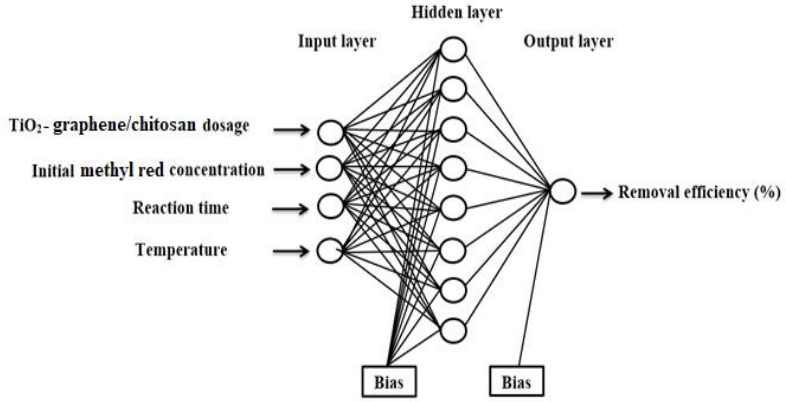

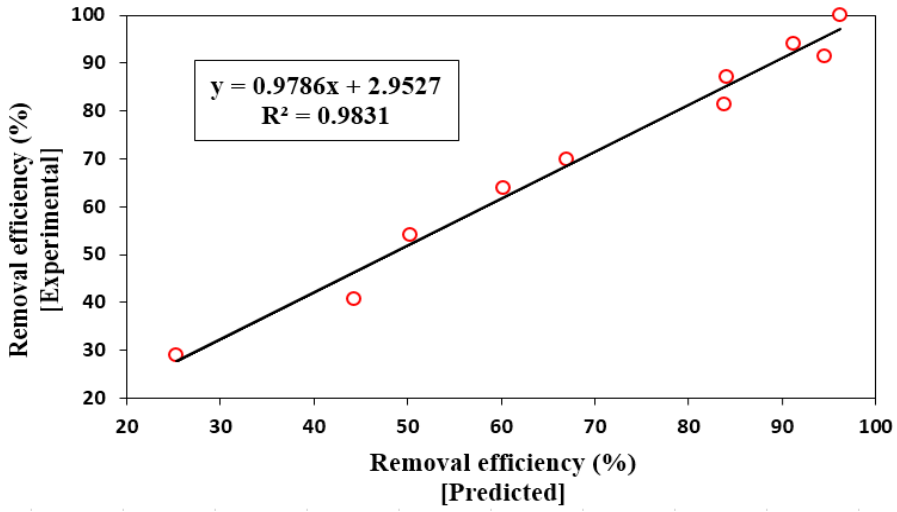

Figure 13. Comparison between ANN predicted and experimental removal efficiency (%) values for the test set of methyl red removal

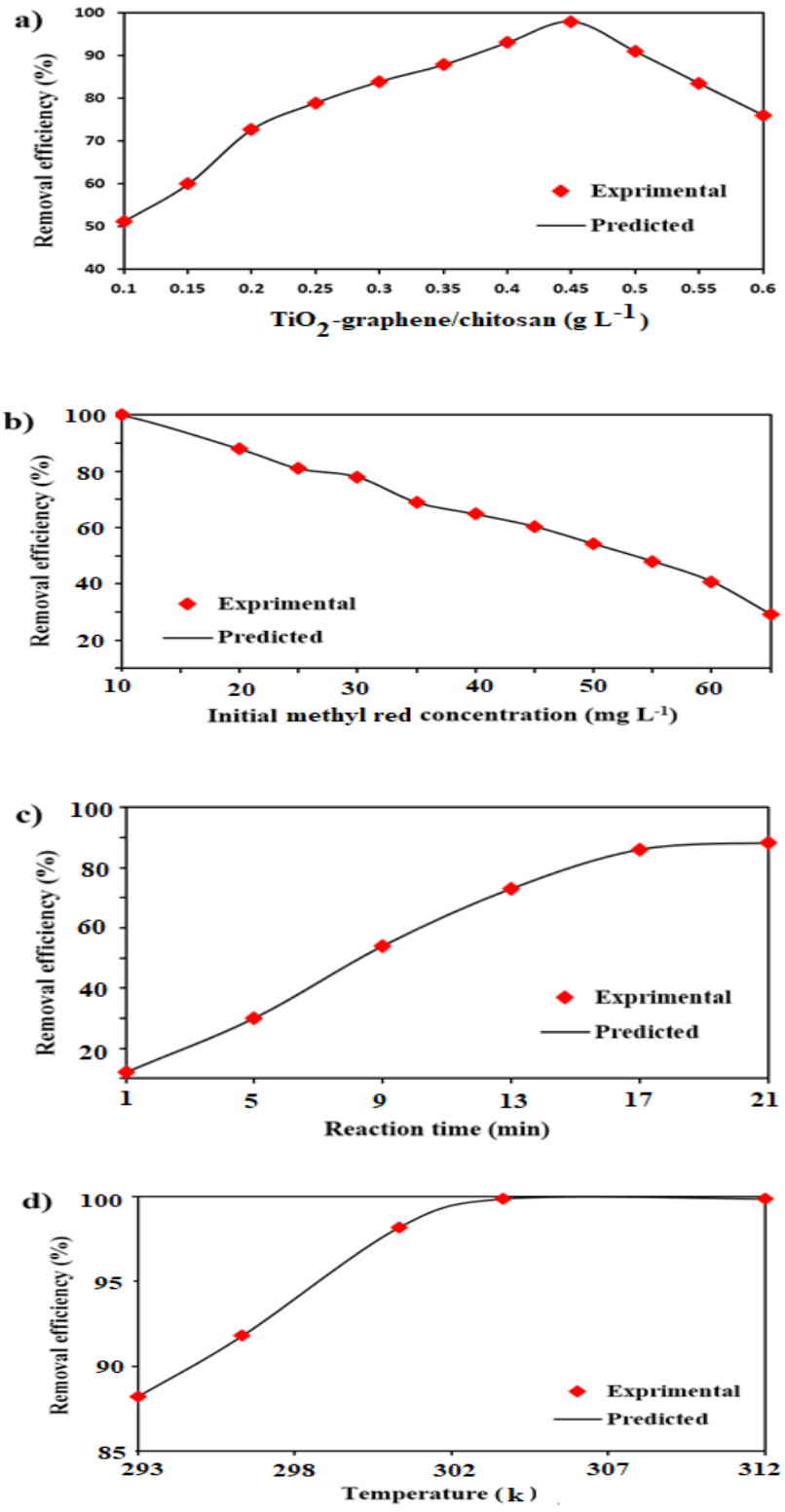

Figure 14. Comparison between ANN predicted and experimental values of methyl red removal efficiency (%) as a function of operational variables: a) catalyst dosage, b) initial dye concentration, c) reaction time and d) temperature

Table 2 represents the weights generated via the ANN models applied in this work for removal of methyl red. The relative importance of the effect of each input variable on output variable can be obtained through the neural weight matrix [49].

For every input variable, the percentage change in the output, as a result of the change in the input variable, was estimated by the following equation 8 [50]:

$$I_j = \frac{\sum_{m=1}^{m=N_h}\left(\left(\left|W_{jm}^{ih}\right| \Big/ \sum_{k=1}^{N_i}\left|W_{km}^{ih}\right|\right)\times\left|W_{mn}^{ho}\right|\right)}{\sum_{k=1}^{k=N_i}\left\{\sum_{m=1}^{m=N_h}\left(\left|W_{km}^{ih}\right| \Big/ \sum_{k=1}^{N_i}\left|W_{km}^{ih}\right|\right)\times W_{mn}^{ho}\right\}} \quad (8)$$

where I_j is the relative importance of the j^{th} input variable on the output variable, N_i and N_h are the number of inputs and hidden neurons, respectively; W's are connection weights, the superscripts 'i', 'h' and 'o', respectively, refer to input, hidden and output layers; and subscripts 'k', 'm' and 'n', respectively, refer to input, hidden and output neurons. Figure 15 represents a comparison between the relative importances of input variables as calculated by equation 2 on the removal of methyl red. As can be seen, reaction time, with a relative importance of 48 %, appeared to be the most influential parameter on the photocatalytic removal of methyl red. Khataee tested ANN comprising four input variables (Initial pH, initial dye concentration, reaction time and UV light intensity) for removal of C.I. Basic red 46 in the presence of TiO_2. He found that initial dye concentration, with a relative importance of 30.75 %, is the most influential parameter on the photocatalytic removal of C.I. Basic red 46 on immobilized TiO_2 nanoparticles [51].

Conclusion

The present study was performed to synthesize and investigate the efficiency of TiO_2-graphene/chitosan nanocomposite to remove the anionic dye (Methyl red) from aqueous solutions. The results demonstrated that TiO_2-graphene/chitosan nanocomposite is more effective in comparison with TiO_2, and TiO_2-graphene catalysts. Based on the results, removal efficiency was obviously affected by TiO_2-graphene/chitosan dosage, initial dye concentration, reaction time and temperature of the solution. Photocatalysis of methyl red can be explained in terms of the Langmuir–Hinshelwood kinetic model (k_{dye} = 0.85 $(mg/L^{-1})^{-1}$ and k_c = 3.21 $(mg/L^{-1})^{-1}$. The performance of the photocatalytic removal of methyl red was successfully predicted by applying a three-layered neural network with eight neurons in the hidden layer, and using a back-propagation algorithm. Also, a measure of the saliency of the input variables was made based on the connection weights of the neural networks, allowing the analysis of the relative importance of input variables to the value of

the dye removal efficiency. The results confirmed that ANN modelling could effectively reproduce experimental data and predict the behavior of the process.

Table 2. Weight matrix for removal of methyl red: weight between input and hidden layers

	W_1 Input variable					W_2 Output	
Neuron	TiO_2 graphene/ chitosandosage	Initial methyl red concentration	Reaction time	Temperature	Bias	Neuron	Removal efficiency (%)
1	-0.322	-0.789	0.688	-2.145	2.353	1	0.756
2	-0.219	1.428	-1.328	-1.288	-2.422	2	-0.159
3	-1.637	0.152	-1.532	-0.423	-0.87	3	-0.866
4	0.059	-1.391	-0.211	-1.852	0.086	4	-0.275
5	0.006	1.495	-0.919	1.528	-0.258	5	-0.222
6	1.255	1.518	1.318	-0.315	0.906	6	0.392
7	1.268	0.283	-1.375	-1.395	1.945	7	-0.021
8	0.652	0.553	-1.233	1.815	2.372	8	-0.053
						Bias	0.126

W_1 and weights between hidden and output layers W_2 [TiO_2-graphene/chitosan], 0 = 0.45-0.6 g L^{-1}, [methyl red], 0 = 10-65 mg L^{-1}, t = 1-21 min, temperature of solution = 293-312 K, and Removal efficiency (%) = 9.2–100

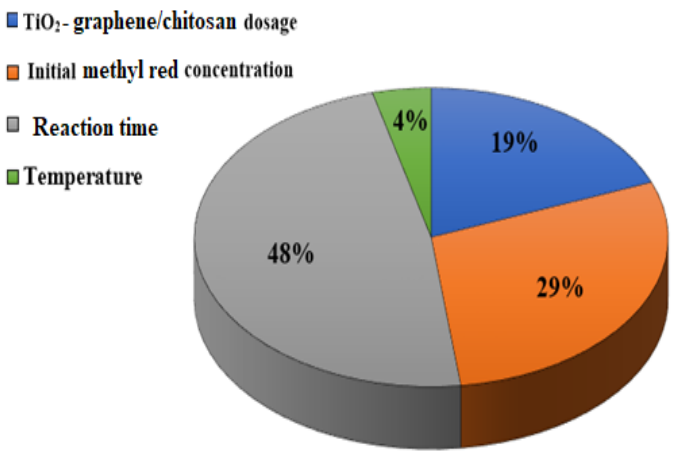

Figure 15. Relative importance (%) of the input a) synthesis and b) operational variables on the removal efficiency (%) values

Acknowledgements

We express our gratitude to the Payame Noor University for supporting this project.

Disclosure Statement

No potential conflict of interest was reported by the authors.

References

[1]. Williams G., Seger B., Kamat P.V. *ACS Nano.,*2008, **2**:1487

[2]. Eckert H., Bobeth M., Teixeira S., Kühn K., Cuniberti G. *Chem. Eng. J.,* 2015, **261**:67

[3]. Martins P.M., Gomez V., Lopes A.C., Tavares C.J., Botelho G., Irusta S., Lanceros-Mendez S. *J. Phys. Chem. C.,* 2014, **118**:27944

[4]. Klymenko N.A., Kozyatnyk I.P., Savchyna L.A.N. *Water. Res.,* 2010, **44**:5316

[5]. Liu X.W., Shen L.Y., Hu Y.H. *Water. Air. Soil. Pollut.* 2016, **227**:141

[6]. Geng W., Liu H., Yao X. *Phys. Chem. Chem. Phys.,* 2013, **15**:6025

[7]. Zhang Y., Zhang N., Tang Z.R., Xu Y.J. *Phys. Chem. Chem. Phys.,* 2012, **14**:9167

[8]. Zhang L., Mohamed H.H., Dillert R., Bahnemann D. *J. Photochem. Photobiol. C: Photochem. Rev.,* 2012, **13**:263

[9]. Zhang H., Lv X., Li Y., Wang Y., Li J. *ACS Nano*., 2010, **4**:380

[10]. Hasan R., Lai C.W., Hamid S.B.A., Basirun W.J., Lockman Z., Bari F. *Eur. Phys. J. Appl. Phys.,* 2014, **65**:20303

[11]. Jiang G., Lin Z., Chen C., Zhu L., Chang Q., Wang N., Wei W., Tang H. *Carbon,* 2011, **49**:2693

[12]. Das B., Choudhury B., Gomathi A., Manna A.K., Pati S.K., Rao C.N.R. *Chem Phys Chem.,* 2011, **12**:937

[13]. Neppolian B., Bruno A., Bianchi C.L., Ashokkumar M. *Ultrason. Sonochem.,* 2012, **19**:9

[14]. Luan T.G., Jin J., Chan S.M.N., Wong Y.S., Tam N.F.Y. *Proc. Biochem.,* 2006, **41**:1560

[15]. Wan Ngah W.S., Teong L.C., Hanafiah M.A.K.M. *Carb. Pol.,* 2011, **83**:1446

[16]. Zhu H.Y., Jiang R., Fu Y.Q., Jiang J.H., Xiao L., Zeng G.M. *Appl. Surface. Sci.,* 2011, **258**:1337

[17]. Mohammadi R., Mohammadi M. *Desalin. Water. Treat.,* 2016, **57**:11317

[18]. Farhangi N., Chowdhury R.R., Medina-GRnzalez Y., Ray M.B., Charpentier P.A. *Appl. Catal. B: Environ.,* 2011, **110**:25

[19]. Mohammadia R., Massoumia B., Emamalinasabba B., Eskandarloo H. *Desalin. Water Treat.,* 2017, **82**:81

[20]. Darvishi Cheshmeh Soltani R., Khataee A.R., Safari M., Joo S.W. *Int. Biodeterior. Biodegradat.,* 2013, **85**:383

[21]. Mohammadia R. *Desalin. Water Treat.*, 2017, **57**:22370

[22]. Demircivi P., Simsek E.B. *Water. Sci. Technol*. 2018, **78**:487

[23]. Loh K.P., Bao Q., Eda G., Chhowalla M. *Nat. Chem.,* 2010, **2:**1015

[24]. Shahabuddin S., Sarih N.M., Kamboh M.A., Nodeh H.R., Mohamad S. *Polym.,* 2016, **8**:305

[25]. Nawi M.A., Jawad A.H., Sabar S., Wan Ngah W.S. *Desalination.,* 2011, **280**:288

[26]. Hasmath Farzana M., Meenakshi S. *Ind. Eng. Chem. Res.,* 2014, **53**:55

[27]. Martinsa P.M., Ferreiraa C.G., Silvaa A.R., Magalhãesa B., Alvesb M.M., Pereirab L. *Composites Part B*., 2018, **145**:39

[28]. Morais A., Longo C., Araujo J.R., Barroso M., Durrant J.R., Nogueira A.F. *Phys. Chem. Chem. Phys.,* 2016, **18**:2608

[29]. Dubey P.K., Tripathi P., Tiwari R.S., Sinha A.S.K., Srivastava O.N. *Int. J. Hydrog. Ene.,* 2014, **39**:16282

[30]. Baran W., Adamek E., Makowski A. *Chem. Eng. J.,* 2008, **145**:242

[31]. Zhang Y.H., Tang Z.R., Fu X.Z., Xu Y.J. *ACS Nano.* 2010, **4**:7303

[32]. Zhang T., Oyama T., Horikoshi S., Hidaka H., Zhao J., Serpone N. *Sol. Energy. Mater. Sol. Cells.,* 2002, **73**:287

[33]. Daneshvar N., Salari D, Khataee A.R. *J. Photochem. Photobiol. A.,* 2004, **162**:317

[34]. Sohrabi M.R., Ghavami M. *J. Hazard. Mater.,* 2008, **153**:1235

[35]. Mohammadia R., Eskandarloo H., Mohammadia M. *Desalin. Water Treat.,* 2015, **55**:1922

[36]. Zhou X.J., Guo W.Q., Yang S.S., Zheng H.S., Ren N.Q. *Bioresource Technol.* 2013, **128**:827

[37]. Okuşluk F., Emre F.B. *Turk. J. Chem.*, 2016, **40**:28

[38]. Mohammadi R., Massoumi B. *Russ. J. Phys. Chem. A.,* 2014, **88**:1184

[39]. Naumenko D., Snitka V., Snopok B., Arpiainen S., Lipsanen H. *Nanotechnology.,* 2012, **23**:465703

[40]. Mahyar A., Behnajady M.A., Modirshahla N. *Ind. J. Chem.,* 2010, **49**:1593

[41]. Marandi R., Olya M.E., Vahid B., Khosravi M., Hatami M. *Environ. Eng. Sci.,* 2012, **29**:957

[42]. Mohammadi R., Massoumi B., Rabani M. *Int. J. Photoenergy,* 2012, 2012:**11** pages

[43] Mohammadi R., Massoumi B., Eskandarloo H. *Desalin. Water Treat.,* 2015, **53**:1995

[44]. Wang J., Li C., Zhuang H., Zhang J. *Food Control.,* 2013, **34**:372

[45]. Mozia S., Morawski A.W., Toyoda M., Inagaki M. *Desalination,* 2009, **241**:97

[46]. Mills A., Morris S. *J. Photochem. Photobiol. A*., 1993, **71**:75

[47]. Aleboyeh A., Kasiri M.B., Olya M.E., Aleboyeh H. *Dyes Pigm.,* 2008, **77**:288

[48]. Kasiri M.B., Aleboyeh H., Aleboyeh A. *Environ. Sci. Technol.,* 2008, **42**:7970

[49]. Daneshvar N., Khataee A.R., Djafarzadeh N. *J. Hazard. Mater.,* 2006, **137**:1788

[50]. Salari D., Daneshvar N., Aghazadeh F., Khataee A.R. *J. Hazard. Mater.,* 2005, **125**:205

[51]. Konstantinou I.K., Albanis T.A. *Appl. Catal. B.*, 2004, **49**:1

How to cite this manuscript: Robab Mohammadi*, Nasrin Sabourmoghaddam. TiO_2-graphene/ chitosan nanocomposite: preparation and its application for removal of anionic dyes. *Asian Journal of Green Chemistry*, 4(1) 2020, 11-32. DOI: 10.33945/SAMI/AJGC/2020.1.2